PROCEEDINGS OF SPIE

SPIEDigitalLibrary.org/conference-proceedings-of-spie

Simultaneous visualization of nerves and blood vessels with multispectral photoacoustic imaging for intraoperative guidance of neurosurgeries

Michelle T. Graham, Joanna Y. Guo, Muyinatu A. Lediju Bell

Michelle T. Graham, Joanna Y. Guo, Muyinatu A. Lediju Bell, "Simultaneous visualization of nerves and blood vessels with multispectral photoacoustic imaging for intraoperative guidance of neurosurgeries," Proc. SPIE 10868, Advanced Biomedical and Clinical Diagnostic and Surgical Guidance Systems XVII, 108680R (26 February 2019); doi: 10.1117/12.2508167

SPIE.

Event: SPIE BiOS, 2019, San Francisco, California, United States

Simultaneous visualization of nerves and blood vessels with multispectral photoacoustic imaging for intraoperative guidance of neurosurgeries.

Michelle T. Graham[a], Joanna Y. Guo[b,c], and Muyinatu A. Lediju Bell[a,b,c]

[a]Department of Electrical and Computer Engineering, Johns Hopkins University, Baltimore, United States
[b]Department of Biomedical Engineering, Johns Hopkins University, Baltimore, United States
[c]Department of Computer Science, Johns Hopkins University, Baltimore, United States

ABSTRACT

Real-time intraoperative guidance during neurosurgeries are often limited to endoscopy or microscopy, which are suboptimal when locating underlying blood vessels and nerves. However, accidental damage to these hidden yet critical structures can have severe surgical complications. To overcome this challenge, we are developing a fast-tuning, multispectral photoacoustic approach to guiding neurological procedures. An *ex vivo* porcine sciatic nerve and *ex vivo* caprine carotid artery perfused with whole human blood were suspended in a water bath. A spectroscopic analysis with wavelengths 690 nm to 1260 nm was performed on each specimen with a constant optical energy of 1.5 mJ/pulse and 11 mJ/pulse utilizing a 1 mm diameter optical fiber and a 5 mm diameter fiber bundle, respectively. The contrast and signal-to-noise ratio of each target was calculated from photoacoustic images, with wavelength-dependent contrast values and signal-to-noise ratios that ranged from 0.41 to 21.8 dB and 10.12 to 25.6 dB, respectively. In particular, the blood vessel contrast (18.2 dB) was greater than the nerve contrast (0.61 dB) when excited with 750 nm light. However, the nerve contrast (10.7 dB) was greater than the blood vessel contrast (6.6 dB) when excited with 1230 nm light. These results indicate that simultaneous visualization of major vessels and nerves requires an imaging system that exploits the unique optical absorption peaks of both hemoglobin and lipids by fast-tuning between two excitation wavelengths (e.g., 750 and 1230 nm).

1. INTRODUCTION

Intraoperative guidance during neurosurgeries has great potential to minimize iatrogenic complications and provide patients with a high standard of care.[1–3] Of particular interest to surgeons are guidance systems that enable the identification of critical structures surrounding the surgical site, such as blood vessels and nerves.[3–5] Accurate identification of these structures prevents damage and associated surgical complications, such as blindness, stroke, fistula, paralysis, and death.[6–8] The ability to differentiate between critical nerves and blood vessels is an additional feature that would be of interest to surgeons, as elastic blood vessels have a higher damage threshold for temporary mechanical stress than nerves, a characteristic which surgeons can use to their advantage when manipulating the surgical field.[9,10]

Current intraoperative image-guidance systems include CT imaging, MR imaging, CT-MR fusion, fluoroscopy, endoscopy, and ultrasonography. Pre-operative CT and MR images provide high resolution anatomical information for precise surgical planning, but can become inaccurate as anatomy is disrupted during surgery. Technological advancements have enabled intraoperative CT and MR imaging, but both require additional safety measures, can disrupt surgical workflow, and intraoperative MR in particular requires highly specific MR compatible operating suite equipment.[1] Endoscopy, which is frequently used in minimally invasive neurosurgeries, enables improved panoramic visualization of the surgical field, but is limited to superficial structures and is unable to locate critical tissues hidden by bone, brain matter, or muscle.[11,12] Ultrasound is restricted by similarities in soft tissue echogenicity as well as limited penetration depth due to high attenuation rates through bony structures. Therefore, predominant challenges with current intraoperative techniques include the real-time tracking of structures as they shift during surgery, the smooth integration of guidance systems into the operating room, and visualization and differentiation of underlying structures in the surgical field. Photoacoustic imaging has the potential to address these current challenges.[13]

Advanced Biomedical and Clinical Diagnostic and Surgical Guidance Systems XVII
edited by Anita Mahadevan-Jansen, Warren S. Grundfest, Proc. of SPIE Vol. 10868
108680R · © 2019 SPIE · CCC code: 1605-7422/19/$18 · doi: 10.1117/12.2508167

Photoacoustic imaging relies on the photoacoustic effect in which tissues selectively absorb light based on their inherent optical properties. The subsequent local heating emits acoustic waves which are sensed by a traditional ultrasound receiver.[14] These images have the potential to provide surgeons with information about underlying structures in the surgical field, as previously explored for neurosurgeries,[13] hysterectomies,[15] and teleoperated surgeries performed with a da Vinci robot.[16,17] The unique optical absorption spectra of different tissues can be leveraged to classify and differentiate between them in a photoacoustic image, despite their similar echogenicity in ultrasound imaging.[18,19] For example, blood vessels and nerves are difficult to differentiate in ultrasound images. However, hemoglobin, the oxygen carrying protein in blood, has an optical absorption peak at 750 nm whereas lipids, a major component of the myelin sheath enveloping nerve axons, has an optical absorption peak at 1230 nm.[20] By alternating the wavelength of the illuminating light, blood vessels and nerves can be differentiated as well as selectively imaged with high contrast.[21–23]

The proposed photoacoustic imaging technique can be incorporated into the operating room with minimal disruption to the surgical workflow. To achieve this goal, a novel light delivery system may be integrated with existing surgical tools[15,24,25] and traditional, portable ultrasound imaging systems can be synchronized with the light source to receive, process, and display photoacoustic images. Previous work has explored this surgical guidance technique technique for a single wavelength,[13,15,16,24] which is sufficient for blood visualization, but not for simultaneous visualization and discrimination of blood vessels and nerves. Therefore, we are exploring the potential of a fast-tuning, multispectral photoacoustic approach to guide head and neck surgeries. This paper reports our spectroscopic analyses to determine the required fast-tuning wavelengths to enable simultaneous visualization of and differentiation between blood vessels and nerves in photoacoustic images.

2. METHODS

Photoacoustic and ultrasound channel data were acquired with an Alpinion (Bothell, WA) E-Cube 12R scanner connected to an Alpinion L3-8 linear array transducer. Two light delivery methods (a 1 mm-diameter optical fiber and a 5 mm-diameter fiber bundle) were individually coupled to an optical parametric oscillator (OPO) driven by a Q-switched Nd:YAG laser operating at 10 Hz with a 10 ns pulse width (Opotek, Inc., Carlsbad, CA). The OPO is capable of generating signal and idler wavelengths in the range 690 - 950 nm and 1200 - 2400 nm, respectively.

A caprine carotid artery was perfused with whole human blood via injection with a syringe and tying off the lumen. The perfused artery and a porcine sciatic nerve, both measuring approximately 5 mm in diameter, were individually suspended in a water bath. The transducer was positioned to visualize the circular cross section of each isolated specimen, as shown in Fig. 1.

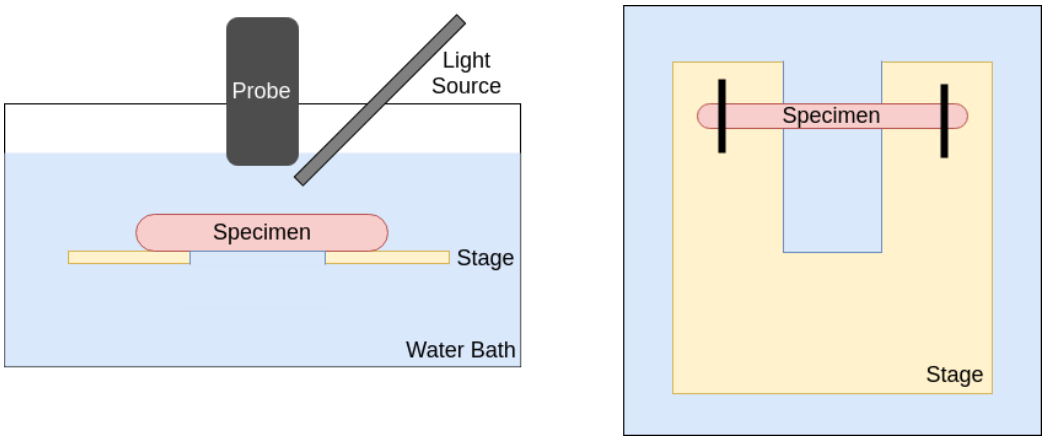

Figure 1. Diagram of experimental setup showing the side (left) and top (right) views of a specimen suspended on a stage in a water bath. The specimen was secured to the stage with string. The ultrasound probe placed with its imaging plane viewing a circular cross-section of the *ex vivo* specimen. The light source was oriented to emit a beam that intersected the ultrasound image plane.

A spectroscopic analysis with wavelengths 690 nm - 800 nm and 1200 nm - 1260 nm was performed on each specimen. The sciatic nerve was illuminated with the 1 mm-diameter optical fiber operating at a constant 1.25 mJ/pulse. The perfused blood vessel was illuminated with the 5 mm-diameter fiber bundle operating at a constant 11 mJ/pulse.

Photoacoustic and ultrasound images were created with delay-and-sum beamforming. Photoacoustic images of each specimen were normalized by the brightest pixel value obtained across all images of the spectroscopic analysis for that specimen. Ultrasound images were normalized by the brightest pixel within that image. The co-registered ultrasound images were used to provide the ground truth location of each specimen.

The contrast and signal-to-noise ratio (SNR) of each target were calculated from photoacoustic data processed with delay-and-sum beamforming. Contrast and SNR were defined as:

$$\text{Contrast} = 20\log_{10}\left(\frac{\mu_t}{\mu_b}\right), \tag{1}$$

$$\text{SNR} = 20\log_{10}\left(\frac{\mu_t}{\sigma_b}\right), \tag{2}$$

where μ_t is the mean within a region of interest (ROI) encompassing the photoacoustic signal of the specimen and μ_b and σ_b are the mean and standard deviation within a ROI representing the photoacoustic signal of the background (i.e. water bath). Each specimen ROI and corresponding background ROI had equivalent areas and were centered at the same image depths. The ROI areas were 5.23 mm^2 and 1.4 mm^2 for the blood vessel and nerve specimens, respectively.

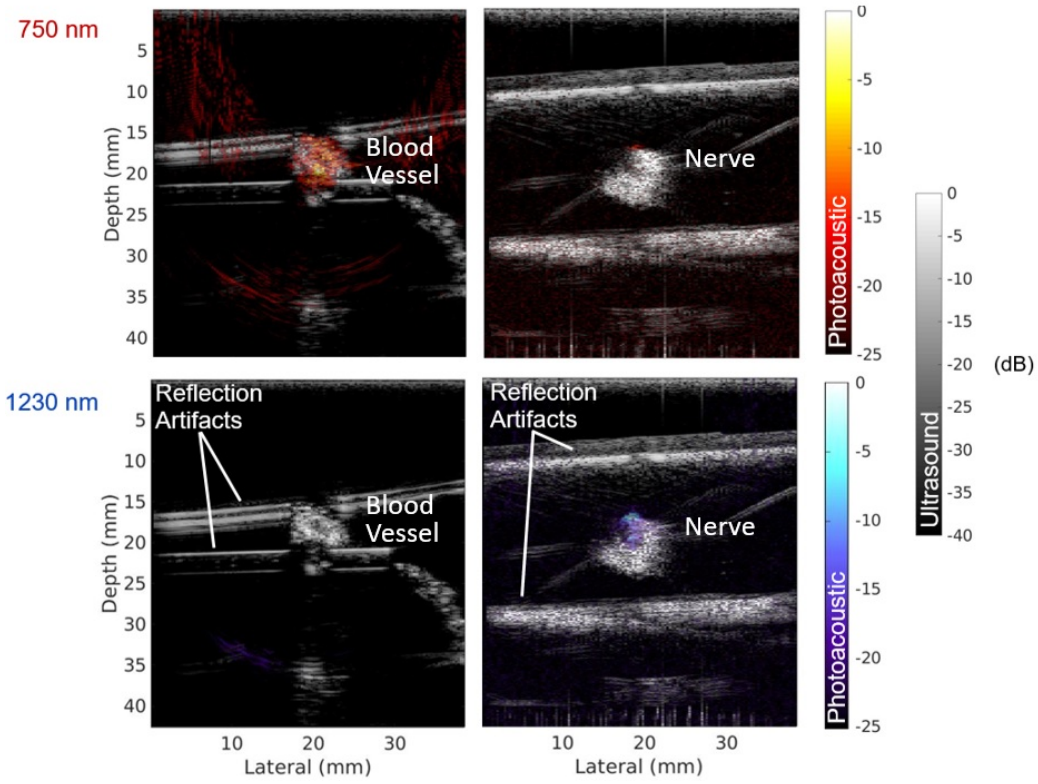

Figure 2. Photoacoustic images of the perfused carotid artery (left) and sciatic nerve (right) superimposed on the co-registered ultrasound images. Photoacoustic images of each specimen were normalized by the brightest pixel value obtained across all images of the spectroscopic analysis for that specimen.

3. RESULTS

Fig. 2 shows log-compressed photoacoustic images of the perfused blood vessel and nerve superimposed on the co-registered ultrasound images. The high amplitude lines in the ultrasound images are reflection artifacts from the acrylic specimen stage. When excited with 750 nm and 1230 nm light, the blood vessel contrast was 18.2 dB and 6.6 dB, respectively. Thus, the photoacoustic images of the blood vessel have 11.6 dB higher contrast at the lower wavelength. The photoacoustic images of the nerve exhibit an opposite trend. When excited with 750 nm and 1230 nm light, the nerve contrast was 0.6 dB and 10.7 dB, respectively. Thus, the photoacoustic images of the nerve have 10.1 dB higher contrast at the higher wavelength.

To provide performance metrics at a wider range of wavelengths, Figs. 3(a) and 3(b) show the measured contrast and SNR, respectively, of the photoacoustic images of each *ex vivo* specimen as a function of wavelength. The perfused blood vessel consistently has higher contrast (18 - 21.8 dB) than the nerve (0.41 - 7.9 dB) when excited with light in the range of 690 nm - 800 nm. However, the nerve contrast (9.4 - 11.4 dB) was consistently greater than the blood vessel contrast (4.1 - 6.6 dB) when exited with light in the range of 1200 nm - 1260 nm. The SNR measurements demonstrate a similar trend. In particular, blood vessel SNR was maximized (21.8 - 25.6 dB) in the lower wavelength range, whereas nerve SNR was maximized (18.6 - 22.1 dB) in the higher wavelength range. In addition, the nerve contrast and SNR exhibit a peak in the lower wavelength range at 775 nm, which is consistent with the peak observed in the optical absorption spectrum of fat. These contrast and SNR measurements demonstrate that photoacoustic image contrast and SNR are maximized for blood vessel and nerves in distinctly different wavelength ranges, i.e. 690 - 800 nm and 1200 - 1260 nm, respectively.

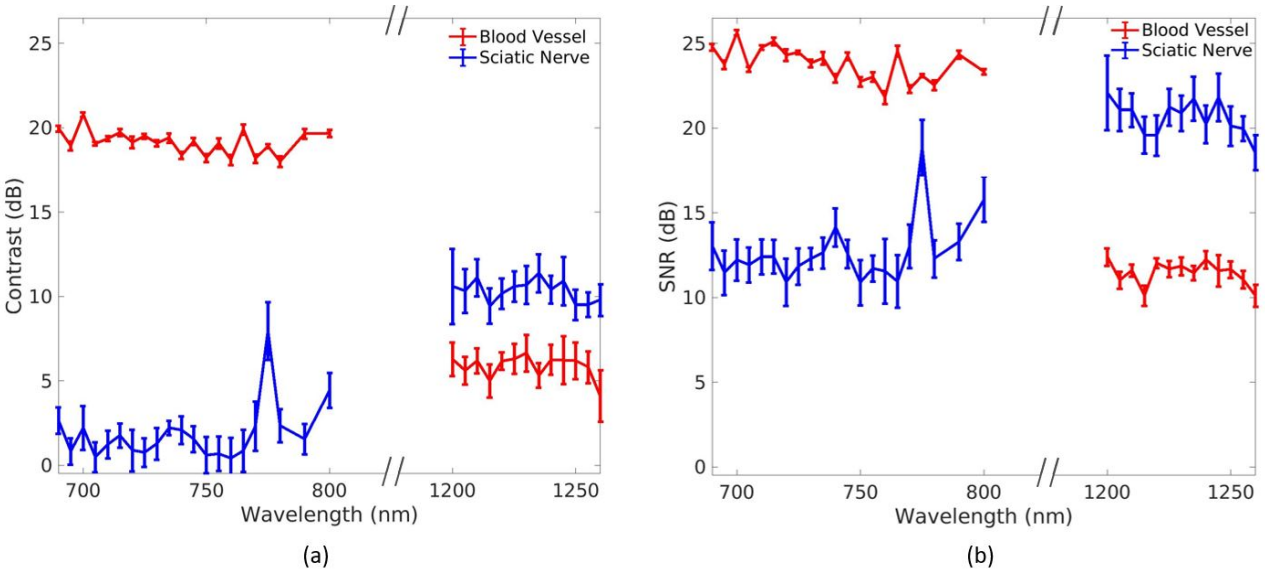

Figure 3. (a) Contrast and (b) SNR measurements calculated from photoacoustic delay-and-sum images as a function of illuminating wavelength for the perfused carotid artery and sciatic nerve. The double slashes on x-axis represent an axis break at wavelengths were no data were collected (800 - 1200 nm).

4. DISCUSSION

This work investigates the excitation wavelengths necessary to distinguish blood vessels from nerves in photoacoustic images. We performed a spectroscopic analysis on each of these tissues. The spectroscopic analyses in Fig. 3 are well correlated with the optical properties of hemoglobin and lipids.[20] As shown in Fig. 2, the photoacoustic image amplitude was higher for the blood vessel when excited with 750 nm and higher for the nerve when excited with 1230 nm light.

Quantitative metrics of contrast and SNR as a function of wavelength further demonstrate the tissue-specific relationships between excitation wavelength and image quality. The blood vessel exhibited its maximum contrast

and SNR in the lower wavelength range of the spectroscopic analysis (690 nm - 800 nm) whereas the nerve exhibited its maximum contrast and SNR in the higher wavelength range (1200 nm - 1260 nm).

An ideal photoacoustic imaging system would alternate between wavelengths of approximately 750 nm and 1230 nm in order to identify critical blood vessels and nerves during surgery. By alternating the wavelength of the excitation light, blood vessels and nerves can be selectively imaged with 18 - 21.8 dB and 9.4 - 11.4 dB contrast, respectively, and 21.8 - 25.6 dB and 18.6 - 22.1 dB SNR, respectively. Future work includes building a fast-tuning system that alternates between these two wavelengths and developing a new display format that would be helpful to a surgeon who needs accurate, real-time information about where to make an incision during surgery to avoid accidental injury to nerves and blood vessels.

5. CONCLUSION

To the authors' knowledge, this work is the first to quantify and compare the visualization of photoacoustic signals from *ex vivo* blood vessel and nerve specimens when excited with wavelengths in two different near infrared (NIR) windows: (1) 690 - 800 nm (which resides in the common NIR-I window) and (2) 1200 - 1260 nm (which resides in the NIR-II window). In order for a surgeon to intraoperatively and simultaneously locate these underlying structures within a surgical field in real-time, a fast-tuning photoacoustic imaging system would be beneficial. With such a system, photoacoustic imaging has strong potential to be used as a real-time intraoperative imaging technique in neurosurgeries to aid in the reduction of iatrogenic injuries to vessels and nerves.

Acknowledgments

This work is supported by NIH R00-EB018994 and an NSF Graduate Research Fellowship. The authors thank Nicholas Louloudis, Sarah Beck, Sue Eller, and Ivan George for their assistance with acquiring the porcine specimens.

REFERENCES

[1] Haberland, N., Ebmeier, K., Hliscs, R., Grunewald, J. P., Silbermann, J., Steenbeck, J., Nowak, H., and Kalff, R., "Neuronavigation in surgery of intracranial and spinal tumors," *Journal of Cancer Research and Clinical Oncology* **126**, 529–541 (Aug 2000).

[2] Wagner, W., Gaab, M. R., Schroeder, H. W. S., and Tschiltschke, W., "Cranial neuronavigation in neurosurgery: Assessment of usefulness in relation to type and site of pathology in 284 patients," *Minimally Invasive Neurosurgery* **43**(3), 124–131 (2000).

[3] Aydn, E., Gk, M., Esenkaya, A., Cinar, C., and Oran, I., "Endovascular management of iatrogenic vascular injury in craniocervical region," *Turkish Neurosurgery* **28** (07 2016).

[4] Sure, U., Alberti, O., Petermeyer, M., Becker, R., and Bertalanffy, H., "Advanced image-guided skull base surgery," *Surgical Neurology* **53**(6), 563 – 572 (2000).

[5] Antoniadis, G., Kretschmer, T., Pedro, M. T., Knig, R. W., Heinen, C., and Richter, H.-P., "Iatrogenic nerve injuries," *Dtsch Arztebl International* **111**(16), 273–279 (2014).

[6] Gordon, S. L., III, W. P. G., Black, J. T., and Miller, S. H., "Accessory Nerve Function After Surgical Procedures in the Posterior Triangle," *Archives of Surgery* **112**, 264–268 (03 1977).

[7] Perry, M., Snyder, W., and Thal, E., "Carotid artery injuries caused by blunt trauma," *Annals of Surgery* **192**(1), 74–77 (1980).

[8] J. Raymond, J. Hardy, R. C. and Roy, D., "Arterial injuries in transsphenoidal surgery for pituitary adenoma; the role of angiography and endovascular treatment," *American Journal of Neuroradiology* **18**(4), 655665 (1997).

[9] Dillavou, E. D., Anderson, L. R., Bernert, R. A., Mularski, R. A., Hunter, G. C., Fiser, S. M., and Rappaport, W. D., "Lower extremity iatrogenic nerve injury due to compression during intraabdominal surgery," *The American Journal of Surgery* **173**(6), 504 – 508 (1997).

[10] Rempel, D., Dahlin, L. B., and Lundborg, G., "Pathophysiology of nerve compression syndromes: Response of peripheral nerves to loading," *The Journal of bone and joint surgery. American volume* **81**, 1600–10 (12 1999).

[11] Kitazawa, K., Okudera, H., Takemae, T., and Kobayashi, S., "Ct guided transsphenoidal surgery: report of nine cases," *Neurological surgery* **21**(2), 147–152 (1993).

[12] Cappabianca, P., Alfieri, A.and Colao, A., Cavallo, L. M., Fusco, M., Peca, C., Lombardi, G., and de Divitiis, E., "Endoscopic endonasal transsphenoidal surgery in recurrent and residual pituitary adenomas: Technical note," *Minimally Invasive Neurosurgery* **43**, 38–43 (2000).

[13] Bell, M. A. L., Ostrowski, A. K., Li, K., Kazanzides, P., and Boctor, E. M., "Localization of transcranial targets for photoacoustic-guided endonasal surgeries," *Photoacoustics* **3**(2), 78 – 87 (2015).

[14] Beard, P., "Biomedical photoacoustics," *Interface Focus* **1**(4), 602–631 (2011).

[15] Allard, M., Shubert, J., and Bell, M. A. L., "Feasibility of photoacoustic-guided teleoperated hysterectomies," *Journal of Medical Imaging* **5**(9) (2018).

[16] Gandhi, N., Allard, M., Kim, S., Kazanzides, P., and Bell, M. A. L., "Photoacoustic-based approach to surgical guidance performed with and without a da vinci robot," *Journal of Biomedical Optics* **22**(12) (2017).

[17] Kim, S., Gandhi, N., Bell, M. A. L., and Kazanzides, P., "Improving the safety of telerobotic drilling of the skull base via photoacoustic sensing of the carotid arteries," *2017 IEEE International Conference on Robotics and Automation (ICRA)* , 2385–2390 (2017).

[18] Mari, J. M., West, S., Beard, P. C., and Desjardins, A. E., "Multispectral photoacoustic imaging of nerves with a clinical ultrasound system," *Proc.SPIE* **8943**(7) (2014).

[19] Horiguchi, A., Tsujita, K., Irisawa, K., Kasamatsu, T., Hirota, K., Kawaguchi, M., Shinchi, M., Ito, K., Asano, T., Shinmoto, H., Tsuda, H., and Ishihara, M., "A pilot study of photoacoustic imaging system for improved real-time visualization of neurovascular bundle during radical prostatectomy," *The Prostate* **76**(3), 307–315 (2016).

[20] Hui, J., Li, R., Phillips, E. H., Goergen, C. J., Sturek, M., and Cheng, J.-X., "Bond-selective photoacoustic imaging by converting molecular vibration into acoustic waves," *Photoacoustics* **2**, 11 – 21 (2016).

[21] Li, R., Phillips, E., Wang, P., Goergen, C. J., and Cheng, J.-X., "Label-free in vivo imaging of peripheral nerve by multispectral photoacoustic tomography," *Journal of Biophotonics* **9**(1-2), 124–128 (2016).

[22] Mari, J. M., Xia, W., West, S. J., and Desjardins, A. E., "Interventional multispectral photoacoustic imaging with a clinical ultrasound probe for discriminating nerves and tendons: an ex vivo pilot study," *Journal of Biomedical Optics* **20**(4) (2015).

[23] Xia, W., Nikitichev, D. I., Mari, J. M., West, S. J., Pratt, R., David, A. L., Ourselin, S., Beard, P. C., and Desjardins, A. E., "Performance characteristics of an interventional multispectral photoacoustic imaging system for guiding minimally invasive procedures," *Journal of Biomedical Optics* **20**(10) (2015).

[24] Eddins, B. and Bell, M. A. L., "Design of a multifiber light delivery system for photoacoustic-guided surgery," *Biomedical Optics Express* **22** (2017).

[25] Shubert, J. and Bell, M. A. L., "A novel drill design for photoacoustic guided surgeries," *Proc. of SPIE, Photons Plus Ultrasound: Imaging and Sensing* **10494** (2018).